

Astronomy Letters, 1996, V.22, N.10 (in press)

Scattering of X-ray emission lines by the neutral and molecular hydrogen in the Sun's atmosphere and in the vicinity of active galactic nuclei and compact sources

R.Sunyaev^{1,2} E.Churazov¹

¹Space Research Institute (IKI), Profsouznaya 84/32, Moscow 117810, Russia

²MPI fur Astrophysik, Karl-Schwarzschild-Strasse 1, 86740 Garching bei Munchen, Germany

arXiv:astro-ph/9608114v1 19 Aug 1996

Abstract

In many astrophysical objects an account for scattering of the X-ray fluorescent and resonance lines of iron ions by the electrons, bound in atomic and molecular hydrogen is important. Specific distortions of the scattered line profile spectrum appear in comparison with scattering by free electrons. Analysis of scattered line spectra may provide information on the ionization state, helium abundance and geometry of scattering media in the vicinity of AGNs, compact X-ray sources and on the surface of X-ray flaring stars and the Sun.

1. Introduction

Compton scattering of X-rays by free electrons is known to play an important role in a number of astrophysical objects: early Universe, hot gas in clusters of galaxies, accretion disks around neutron stars and black holes, plasma clouds surrounding compact X-ray sources. In many cases X-rays are scattered by neutral gas rather than free electrons. One can mention the reflection of X-rays by the solar photosphere (X-rays are produced by the flares above the solar surface and a considerable fraction of them will be reflected by the photosphere, having low degrees of ionization $\frac{e}{H} \leq 10^{-3}$); reflection of X-rays by the photospheres of cold flaring stars (T-Tauri, late stars coronas); outer regions of the extended accretion disks in binary systems, having low degree of ionization; molecular tori around central objects in the active galactic nuclei and QSOs. Compact X-ray sources, embedded into the dense molecular clouds are of special interest. Discovery of the giant molecular cloud in the direction of the source 1E1740.7–2942 (Bally and Leventhal 1991) indicates that the source is possibly surrounded by the dense molecular gas. Provided the strong variability of the compact source, observations of scattered component (leaving the cloud with substantial time lag) are possible, allowing one to study the parameters of the molecular cloud by means of X-ray astronomy methods.

Sunyaev, Markevitch and Pavlinsky (1993) have noted that strong concentration of the molecular hydrogen in the giant clouds in the Galactic Center region should lead to the appearance of the diffuse emission, related to the scattering of the compact X-ray sources and Sgr A* by the molecular hydrogen in these clouds. It was also noted, that detection of a strong fluorescent line of neutral iron ($h\nu = 6.4$ keV) and characteristic spectrum of scattered component may provide unique information on the activity of this region during last several hundreds years. Moreover, scattering of the emission from the nucleus of the Galaxy by the neutral and molecular cloud of the whole Galaxy should lead to the appearance of the diffuse component, which contains the information of the activity of the nucleus during past tens of thousands of years. Recent ASCA observations of the diffuse emission of the Galactic Center region (Koyama, 1994) gave new information in support of this hypothesis. Along with emission lines from the hydrogen- and helium-like ions of heavy elements, the powerful iron fluorescent line (K_α) was detected, which surface brightness distribution roughly follows the distribution of giant molecular clouds. In particular the molecular complex Sgr B2 was found to be especially bright in this line.

Bolometric observations with high energy resolution (better than 10 eV) of ASTRO-E, Bragg spectrometer (resolution \sim eV) of Spectrum-X-Gamma and gratings of XMM and AXAF can verify another prediction – specific shape of the low energy wing of the lines formed due to scattering by atomic or molecular hydrogen. The shape of the low energy wing is related to the recoil effect and contains the information on the geometry of scattering. We will show below that recoil effect on bound electrons differs substantially from that on the free electrons. Thus, the spectral shape of the scattered line can be used as diagnostic of the ionization balance in the scattering medial in distant AGNs and QSOs. Moreover studying shapes of the scattered lines opens the principal possibility of helium

abundance determination at the Sun's surface and in molecular clouds.

Major effects are the *smearing of back scattering peak and appearance of the energy gap* – lack of photons in the interval from initial photon energy $h\nu_0$ down to $h\nu_0 - E$, where E is the excitation energy of the first levels above ground level ($E = 10.2$ eV for atomic hydrogen, $E \approx 20$ eV for neutral helium, $E = 40.8$ eV for He II ion, $E \approx 11$ eV for molecular hydrogen). The possibility of the detection of Raman satellites of X-ray emission lines is very attractive. The energies of these lines are shifted by the excitation energy of various levels of the atoms of hydrogen and helium. Of course with the current X-ray CCD and cooled solid state detectors with an energy resolution about 100 eV one can expect detection of effects only in the zone with $\Delta h\nu \sim 100$ eV. As is shown below these effects are large enough.

2. Scattering by hydrogen atoms

All astrophysicists, dealing with detectors of X and Gamma-ray emission, know that Compton scattering takes place in the neutral gas or solid matter of the detector (e.g. Zombeck 1990). Basko & Sunyaev, 1973 and Basko et al. 1974 for the first time considered in detail the problem of heating the surface of the atmosphere of normal star in the close binary system HZ Her/Her X-1 and mentioned the importance of scattering and reflection of X-rays by the weakly ionized atmosphere of Hz Her. They noted that for the photons with energy above a few keV the recoil effect exceeds the ionization potential of hydrogen. Thus in the first approximation scattering of such photons by neutral hydrogen does not differ from scattering by free electrons. The same approximation was used by Basko, 1978 and George & Fabian, 1991, considering the reflection of X-rays by the stellar surface and cold accretion disk.

The necessity of more detailed treatment arises because of the appearance of the new generation of X-ray instruments with the energy resolution \sim few eV at the fluorescent line 6.4 keV, and resonance lines of hydrogen- and helium-like ions of iron. Below we discuss the effects which can be observed by the instruments which are going to be launched by the year 2000 (Spectrum-X-Gamma with Bragg spectrometer, AXAF and XMM with gratings, ASTRO-E with X-ray bolometers).

Most of the relations describing the process of X-ray photon scattering by free or bound electrons are well known and can be found in the textbooks and original papers. We give some below for completeness.

For the scattering of a photon by a free electron ($\gamma_1 + e_1 = \gamma_2 + e_2$) the frequency of the photon after scattering is unambiguously defined by the geometry of scattering, due to energy and momentum conservation laws:

$$\nu_2 = \nu_1 \frac{1 - \frac{v}{c} \vec{\Omega}_1}{1 - \frac{v}{c} \vec{\Omega}_2 + \frac{h\nu_1}{\gamma m_e c^2} (1 - \vec{\Omega}_1 \vec{\Omega}_2)} \quad (1)$$

where $\vec{\Omega}_1, \nu_1$ and $\vec{\Omega}_2, \nu_2$ characterize the direction and frequency of the photon before and after scattering, \vec{v} is the velocity of the electron before scattering, $\gamma = \frac{1}{\sqrt{1-\frac{v^2}{c^2}}}$, $\vec{\Omega}_1 \vec{\Omega}_2 = \cos\theta$, θ is the scattering angle (see e.g. Kompaneetz, 1956, review of Pozdnyakov et al., 1982).

In the limit $\vec{v} = 0$ and $\frac{h\nu_1}{m_e c^2} \ll 1$ change of the photon energy is related to the recoil effect:

$$\nu_2 = \nu_1 \left[1 - \frac{h\nu_1}{m_e c^2} (1 - \cos\theta) \right] \quad (2)$$

In the limit $\frac{h\nu_1}{m_e c^2} \ll \frac{v}{c}$ Doppler effect dominates:

$$\nu_2 = \nu_1 \frac{1 - \frac{\vec{v} \cdot \vec{\Omega}_1}{c}}{1 - \frac{\vec{v} \cdot \vec{\Omega}_2}{c}} \quad (3)$$

For the scattering by the electron, bound in a hydrogen atom, additional factors complicate the process: finite binding energy of the electron and motion of the electron in the atom. Because of discrete energy levels of the electron in the excited state not all values of photon energy change are possible. Because of the “random” motion of the electron within the atom change of the photon energy is no longer unambiguous function of the geometry. For free electrons Pozdnyakov et al., 1979 noted, that even at rather low electron temperatures $kT_e \sim 1$ eV profile of a scattered line apparently broadens due to the Doppler effect (see e.g. Fig.7 in Pozdnyakov et al., 1982). Note that in this example electron velocity was $v \approx 400$ km/s, the value not unusual for accretion disks in X-ray binary systems and galactic nuclei. Characteristic velocity of the electron in hydrogen atom is $v \sim \alpha c \sim 2000$ km/s ($1/\alpha = \hbar c/e^2 = 137$ is the fine structure constant) and motion with such velocity should significantly affect the amount of energy transferred to the electron during the scattering. This ambiguity of energy transfer does not violate conservation laws, since heavy nucleus can carry the necessary momentum, having negligible kinetic energy.

Depending on the final state of the electron, the scattering process can be divided into three branches:

A) Rayleigh (coherent) scattering: $\gamma_1 + H = \gamma_2 + H$. The energy of the photon remains the same, only direction changes. The recoil effect is $\sim m_p/m_e$ times lower than in the case of scattering by free electron.

B) Raman scattering: $\gamma_1 + H = \gamma_2 + H(n, l)$, where $H(n, l)$ denotes one of the excited states of the hydrogen atom. The energy of the photon decreases by the value of excitation energy: $h\nu_2 = h\nu_1 - E_{n,l}$ – Raman satellites of the line appear.

C) Compton scattering: $\gamma_1 + H = \gamma_2 + e^- + p$, accompanied by ionization of atom. The energy of the photon decreases by the value of ionization potential and kinetic energy of electron after scattering: $h\nu_2 = h\nu_1 - 13.6\text{eV} - E_e$.

It is necessary to mention that in a non-relativistic limit sum over differential crosssections of these three branches is equal to the Thomson differential crosssection (see below).

Below we briefly discuss each of these three processes. More detailed discussion on the process of scattering by hydrogen atom and references for original publications can be found in e.g. Eisenberger & Platzman, 1970.

The following notations will be used throughout the paper:

$\nu_1, \nu_2, \vec{k}_1 = \vec{\Omega}_1 \frac{h\nu_1}{c}, \vec{k}_2 = \vec{\Omega}_2 \frac{h\nu_2}{c}$ are initial and final frequencies and momenta of the photon, $\Delta\nu = \nu_1 - \nu_2, \vec{q} = \vec{k}_1 - \vec{k}_2$ are change of the frequency and momentum, $\vec{\chi} = \vec{q}/\hbar, a = r_b/\hbar, r_b$ – Bohr radius, θ is the scattering angle,

$$\left(\frac{d\sigma}{d\Omega}\right)_{Th} = 0.5 \cdot r_e^2 \cdot (1 + \cos^2\theta) \left(\frac{\nu_2}{\nu_1}\right)^2 \quad (4)$$

is the differential crosssection for scattering of the photon by a free electron at rest in non-relativistic limit. This expression coincides with the familiar expression $\left(\frac{d\sigma}{d\Omega}\right)_{Th} = 0.5 \cdot r_e^2 \cdot (1 + \cos^2\theta)$, except for the factor $\sim \frac{\nu_2}{\nu_1} \approx 1$, which appears in the expression for crosssection when a change of the photon energy can't be neglected. We drop this factor in a few expressions below, which is certainly valid for the considered range of photon energies.

The probability of photon scattering accompanied by the transition of electron from the initial state i to the final state f can be calculated from perturbation theory. The crosssection can be calculated as $\frac{2\pi}{\hbar c} |X|^2 \rho \times \delta(\Delta E - h\nu)$ (e.g Heitler, 1960), where $\rho \approx \frac{k_2^2 d\Omega}{(2\pi\hbar c)^3}$ is the density of the final states per unit energy, ΔE is the change of electron energy. In the first order perturbation theory $X = H'_{if} = \int \psi_f^* H' \psi_i^*$ (e.g. Landau & Lifshitz, 1958, Heitler, 1960). H' in the above expression stands for the term in Hamiltonian responsible for the interaction of the electron and photon. In non-relativistic approximation

$$H' = e^2 A^2 / 2mc^2 - e\vec{p}\vec{A}/mc \quad (5)$$

(e.g. Landau & Lifshitz, 1961, Heitler, 1960), where \vec{A} is the vector-potential of the electromagnetic field, \vec{p} is the momentum of the electron. Scattering of the photon appears in the first order perturbation theory for the term $e^2 A^2 / 2mc^2$ in the expression (5) and in the second order for the term $e\vec{p}\vec{A}/mc$. In the case under consideration (scattering of photons with energy \sim few keV by light elements) the second term in the expression (5) can be neglected (e.g. Heitler, 1960, Eisenberger & Platzman, 1970). Substituting \vec{A} with the plane wave one gets the expression for the matrix element for transition $i \rightarrow f$:

$$H'_{if} = \frac{e^2}{mc^2} (\vec{e}_1 \vec{e}_2) \frac{2\pi\hbar^2 c^2}{\sqrt{h\nu_1 h\nu_2}} \int \psi_f^* e^{i\vec{\chi}\vec{r}} \psi_i = \frac{e^2}{mc^2} (\vec{e}_1 \vec{e}_2) \frac{2\pi\hbar^2 c^2}{\sqrt{h\nu_1 h\nu_2}} \langle f | e^{i\vec{\chi}\vec{r}} | i \rangle \quad (6)$$

\vec{e}_1 and \vec{e}_2 in the above expression stand for the unit vectors in the direction of polarization of the photon before and after scattering. Thus final expression for the differential crosssection of photon scattering with a given change of frequency, direction and polarization will be

as follows:

$$\frac{d\sigma}{d\Omega dh\nu} = \left(\frac{e^2}{mc^2}\right)^2 \left(\frac{\nu_2}{\nu_1}\right) (\vec{e}_1 \vec{e}_2)^2 \sum_f |\langle f | e^{i\vec{x}\vec{r}} | i \rangle|^2 \times \delta(\Delta E_{if} - \Delta h\nu) \quad (7)$$

Summation in the expression (7) is performed over all possible final states of the electron (including continuum). In order to calculate the crossection for each of the channels (Rayleigh, Raman, Compton scatterings) one has to substitute appropriate wave functions in the expression (7). For hydrogen atom calculations can be done analytically. Initial state will always be ground state of hydrogen with wave function $\psi_i = \frac{1}{\sqrt{r_b^3 \pi}} e^{-r/r_b}$. For Rayleigh scattering $\psi_f \equiv \psi_i$. For Raman or Compton scatterings ψ_f corresponds to one of the excited discrete or continuum states of hydrogen respectively.

One can show that for any given angle the total scattering crossection (integrated over all possible energies of the photon in the final state) does not depend on the energy of the initial photon (if factor $\frac{\nu_2}{\nu_1}$ can be replaced with unity):

$$\frac{d\sigma}{d\Omega} = \int \frac{d\sigma}{d\Omega dh\nu} dh\nu \approx r_e^2 (\vec{e}_1 \vec{e}_2)^2 \sum_f |\langle f | e^{i\vec{x}\vec{r}} | i \rangle|^2 = r_e^2 (\vec{e}_1 \vec{e}_2)^2 \sum_f \langle i | e^{i\vec{x}\vec{r}} | f \rangle \langle f | e^{-i\vec{x}\vec{r}} | i \rangle \quad (8)$$

Using the know relation $\sum_f |f\rangle \langle f| = 1$ (e.g. Schiff, 1955) one can show that $\sum_f |\langle f | e^{i\vec{x}\vec{r}} | i \rangle|^2 = \langle i | 1 | i \rangle = 1$. Thus in the considered range of photon energies ($E_b \ll h\nu_1 \ll m_e c^2$), angular distribution of scattered photons will always follow the expression $\frac{d\sigma}{d\Omega} = r_e^2 (\vec{e}_1 \vec{e}_2)^2$ (i.e. the same as for scattering by free electron in Thomson limit). The presence of different final states of electron affects only the spectrum of scattered radiation. Averaging over the polarization directions leads to the appearance of the factor $(1 + \cos^2\theta)$ – i.e. the Rayleigh scattering diagram.

2.1. Rayleigh scattering

a) Hydrogen atom

For Rayleigh scattering the final state of the electron coincides with it's initial (ground) state. The direction of the photon propagation changes, but the frequency remains the same. Motion of the heavy atom as a whole compensates for the change of photon momentum. If the energy of the photon is greater than the binding energy of the electron, but the wavelength is much larger than the characteristic size of the atom then the differential crossection of Rayleigh scattering coincides with that for free electron in the Thomson limit:

$$\frac{d\sigma}{d\Omega} = \left(\frac{d\sigma}{d\Omega}\right)_{Th} \quad (9)$$

For the photons with energies of the order of 1–10 keV the wavelength is comparable with the size of the atom and differential crossection of Rayleigh scattering as follows (e.g.

Eisenberger & Platzman, 1970 with reference to results of Schnait, 1934):

$$\frac{d\sigma}{d\Omega} = \left(\frac{d\sigma}{d\Omega} \right)_{Th} \cdot [1 + (\frac{1}{2}ka)^2]^{-4} \quad (10)$$

From (10) one can see that Rayleigh scattering plays an important role when the change of photon momentum is less than the typical momentum of electron bound in an atom (i.e. $ka \lesssim 1$). For X-ray photons the initial momentum is relatively high and the condition of a small change of momentum means scattering at small angles $\theta \lesssim 1/k_1a$ (see Fig.1). At $ka \gg 1$ Rayleigh crosssection declines as $(ka)^{-8}$. The fast decline of the crosssection at $ka \gg 1$ is due to the rapidly oscillating term in the expression (6).

b) Molecular hydrogen and atomic helium

The important property of Rayleigh scattering is the possibility of coherent scattering of the photon by the electrons, located in the small volume (e.g. in atom) with the characteristic size l . In classical electrodynamics the parameter $x = l \cdot \chi$ (i.e. typical phase shift between waves scattered by different electrons) defines the efficiency of scattering. Intensity of radiation scattered by Z electrons is proportional to

$$\left(\sum_j^Z e^{i\vec{\chi}r_j} \right)^2 \quad (11)$$

Obviously for $x \ll 1$ crosssection will be proportional to Z^2 . In the opposite case of $x \gg 1$ each electron scatters waves independently and the crosssection is simply proportional to Z . Similar behavior remains valid in quantum mechanics. The crosssection for scattering by multi-electron atom is proportional to the expression

$$\sum_f |\langle f | \sum_j^Z e^{-i\vec{\chi}r_j} | i \rangle|^2 = \sum_f \langle i | \sum_m^Z e^{+i\vec{\chi}r_m} | f \rangle \langle f | \sum_n^Z e^{-i\vec{\chi}r_n} | i \rangle = \sum_m \sum_n |\langle i | e^{-i\vec{\chi}(r_n - r_m)} | i \rangle| \quad (12)$$

For $x \ll 1$ factor $e^{-i\vec{\chi}(r_n - r_m)} \approx 1$ at the characteristic scale of atom and the crosssection is proportional to Z^2 . For larger values of x the crosssection is proportional to Z (i.e. to the number of electrons in the atom).

In astrophysical conditions coherent scattering increases the role of elements with $Z > 1$ in comparison with atomic hydrogen (due to the factor Z per electron for small angle scattering). For normal cosmic abundance the contribution of heavy elements is not large: summation over all elements increases the crosssection for forward scattering by a factor ~ 1.4 per hydrogen atom (a similar factor appears in the expression for bremsstrahlung emission of cosmic plasma, which is also proportional to Z^2). The most important correction (about 40%) is due to helium. The increase of the Rayleigh scattering crosssection may be important for the giant molecular clouds, scattering X-ray emission of X-ray sources.

2.2. Raman scattering

For Raman scattering final state of the electron corresponds to one of the excited discrete levels. Accordingly photon changes the energy by the excitation energy of this level. For the hydrogen atom this means that the following values of photon energy decrement are possible: $13.6 \times (1 - 1/n^2)$, where n the is principal quantum number of the excited level. The crosssection (with excitation of level n) is given by Schnait, 1934:

$$\left(\frac{d\sigma}{d\Omega}\right)_n = \left(\frac{d\sigma}{d\Omega}\right)_{Th} \frac{2^8 (ka)^2}{3 n^3} \left[3(ka)^2 + \frac{(n^2 - 1)}{n^2}\right] \frac{[(n - 1)^2/n^2 + (ka)^2]^{n-3}}{[(n + 1)^2/n^2 + (ka)^2]^{n+3}} \quad (13)$$

For X-ray photons contribution of Raman scattering to the total crosssection is never large. For very small angle scattering $ka \ll 1$ crosssection $\left(\frac{d\sigma}{d\Omega}\right)_n \propto (ka)^2$ and Rayleigh scattering dominates, while for scattering at large angles $ka \gg 1$ and the crosssection of Raman scattering decline as $(ka)^{-8}$. Raman scattering gives maximal contibution when $ka \approx 1$, for 6.4 keV photons this corresponds to scattering at ~ 30 degrees.

It is worth mentioning again that for the scattering of a monochromatic line with energy $h\nu_1$ a set of monochromatic lines will appear after the Raman scattering with energies $h\nu_2 = h\nu_1 - \Delta E_n, n = 1, 2, ..$ (see Fig.3). This opens the possibility to observe the energy gap of 10.2 eV (the energy corresponding to the $1s - 2p$ transition in hydrogen) just below the energy of the initial photons. Scattered photons can not appear in this gap because of the energy conservation law.

2.3. Compton scattering

For Compton scattering final state of the electron corresponds to the continuum. For the scattering by a free electron at rest the energy of the scattered photon is unambiguously related to the scattering angle according to (2). For the scattering by a bound electron this unambiguous relations breaks even if the atom or molecule are not moving before scattering. This is because the electron is not “at rest” in the atom, but has certain distribution over momentum. For scattering at large angles (where Compton process dominates) energy transfer is greater than the binding energy of the electron. In such condition scattering process is “fast” compared to the motion of the electron in atom, and the whole process can be described as scattering by free electron having “random” initial momentum, corresponding to electron momentum distribution in hydrogen atom. There is no violation of the momentum conservation law, since heavy nucleus compensate the initial momentum of the electron, without affecting the energy conservation law. Detailed justification of the possibility of such treatment of the scattering process (so called “impulse approximation”) is discussed by Eisenberger & Platzman, 1970. For the free electron one can write:

$$\Delta h\nu = \frac{k^2}{2m} + \frac{\vec{k} \cdot \vec{p}_0}{m} \quad (14)$$

where \vec{p}_0 is the initial momentum of the electron. Note that the first term in the relation (14) corresponds to the usual recoil, and the second corresponds to the Doppler effect.

The broader the distribution of the electron initial momentum, the larger the deviations of energy change (second term in (14)) compared to pure recoil according to expression (2).

Thus for bound electrons momentum distribution in the atom plays the same role as the temperature does for the free electrons. The left (low energy) wing of the line, scattered by free electrons of plasma with temperature ~ 13.6 eV, will resemble the result of scattering by neutral hydrogen (Fig.4).

For hydrogen analytical expression of the differential crosssection is known (Gummel & Lax, 1957, Eisenberger & Platzman, 1970)

$$\frac{d\sigma}{dh\nu d\Omega} = \left(\frac{d\sigma}{d\Omega} \right)_{Th} \left(\frac{\nu_1}{\nu_2} \right) \langle |M_{fi}| \rangle^2 \delta(E_f - E_i - \Delta h\nu) \quad (15)$$

$$\begin{aligned} \langle |M_{fi}| \rangle^2 = & \frac{\pi^2 8^3 a^2}{p} (1 - e^{-2\pi/pa})^{-1} \times \exp\left[\frac{-2}{pa} \arctg\left(\frac{2pa}{1 + k^2 a^2 - p^2 a^2} \right) \right] \times \\ & [k^4 a^4 + \frac{1}{3} k^2 a^2 (1 + p^2 a^2)] \times [(k^2 a^2 + 1 - p^2 a^2)^2 + 4p^2 a^2]^{-3} \end{aligned} \quad (16)$$

$$\text{where } p^2/2m = -|E_b| + \Delta h\nu$$

For many electron atoms one can use “impulse approximation” in the limit of photon energy decrement much larger than the electron binding energy

$$\frac{d\sigma}{dh\nu d\Omega} = \left(\frac{d\sigma}{d\Omega} \right)_{Th} \frac{1}{(2\pi)^3} \int \delta \left(\Delta E - \frac{k^2}{2m} + \frac{\vec{k} \cdot \vec{p}_0}{m} \right) P(\vec{p}_0) d^3 p_0 = \left(\frac{d\sigma}{d\Omega} \right)_{Th} J(\vec{k} \cdot \vec{p}_0) \quad (17)$$

here $P(\vec{p}_0)$ - is the probability to find the electron with \vec{p}_0 in the initial state. Quantity $J(q) = J(\vec{k} \cdot \vec{p}_0)$ is so called Compton profile. One can find extensive tables of $J(q)$ for multi-electron atoms e.g. in Briggs et al. 1975.

At lower energies the role of Rayleigh and Raman scattering increases considerably along with the deviations of the Compton scattering crosssection from the case of a free electron at rest. For example differential crosssections and scattered component spectrum (averaged over all angles) are shown in Fig. 5 for initial photon energy 3.32 keV (this energy corresponds to the resonance line of the hydrogen-like argon). For the spectrum averaged over all angles the fraction of Rayleigh scattering is 36%, about 6% of the scattered photons form the first Raman satellite of the line ($h\nu = h\nu_0 - 10.2$ eV).

2.4. Scattering by molecular hydrogen and atomic helium

2.4.1. Molecular hydrogen

The difference between scattering by molecular and atomic hydrogen is most prominent for scattering by small angles (i.e. for Rayleigh scattering). Firstly, coherent (Rayleigh)

scattering by molecule will be “enhanced” by a factor of Z i.e. a factor of 2 (Fig.2). Secondly the structure of electron terms in the molecule differs somewhat from that in the hydrogen atom. As a result the gap between the unshifted line (due to Rayleigh scattering) and the line corresponding to the Raman scattering with excitation of the first electron term in the molecule will be ~ 11 eV compared to 10.2 eV in atomic hydrogen.

Compton scattering by large angles will be very similar to that for atomic hydrogen. In particular “blurring” of the scattered line profile due to distribution of electron momentum in the initial state will be present. The spectrum of 6.4 keV emission scattered by a hydrogen molecule and averaged over all scattered angles is shown in Fig.6. The data of Eisenberger 1970 on the Compton profile of the H_2 molecule have been used for these calculations. Fig.6 shows that for the existing X-ray detectors scatterings by atomic and molecular hydrogen are almost indistinguishable.

2.4.2. Helium

For the scattering by a helium atom along with the increase of Rayleigh scattering (by a factor of 2) the structure of the lines, corresponding to Raman scattering, changes strongly. In particular the gap between ground and first excited state in the helium atom is ~ 20 eV. Note, that for ~ 6 keV photons the wavelength $\lambda \sim 2\text{\AA}$ is comparable with the size of the atom and the parity selection rule is not strict. Due to the stronger binding of the electron in the helium atom, electron momentum distribution is substantially wider than that in atomic or molecular hydrogen. As a result (see Fig.6) the left wing of the line will be more “blurred”. A comparison of the spectra scattered by hydrogen and helium atoms is given in Fig.6. The energy gap is twice as large as that for the hydrogen atom and significant differences in the recoil profile allow one to hope that studying the recoil spectrum might become a method for helium abundance determination. Note that even after multiple scatterings photon does not appear in this energy gap.

3. Coefficients of transfer

a) Change of energy

The difference in the differential crosssections $\frac{d\sigma}{d\Omega d h\nu}$ for free and bound electrons should be taking into account considering the evolution of spectra in the Fokker-Plank approximation. The Fokker-Plank equation uses the mean energy change and the mean square of energy change of the photon after a large number of scatterings. For free electrons at low temperature the corresponding expressions have been given by Ross et al. 1978: the mean energy change of the photon $A(h\nu) = -n_e\sigma_T c \left(\frac{h\nu}{mc^2}\right) (h\nu)$ and the mean square of the energy change $B(h\nu) = n_e\sigma_T c \frac{7}{5} \left(\frac{h\nu}{mc^2}\right)^2 (h\nu)^2$. Shown in Fig.7 is the dependence of the mean energy change and the square of energy change for scattering by free and bound electrons. The mean energy change practically coincides with that for the free electron at

rest (see e.g. Eisenberger & Platzman, 1970), while the mean square of energy change is larger in the case of scattering by bound electrons. This is due to additional “blurring” of the recoil profile due to distribution of the electron momentum in the initial state. To the order of magnitude the mean square of energy change for scattering by a bound electron is $(h\nu_B)^2 = (h\nu)^2 + h\nu < \frac{p^2}{2m} >$, where $h\nu$ is the recoil for the scattering by free electron. Using the results of Eisenberger & Platzman, 1970 one can write the expression for the mean square of energy change per unit time as :

$$B(h\nu) = n\sigma_T c \left[\frac{7}{5} \left(\frac{h\nu}{mc^2} \right)^2 (h\nu)^2 + \frac{4}{3} (h\nu) \left(\frac{h\nu}{mc^2} \right) 13.6eV \right] \quad (18)$$

The first term in expression (18) corresponds to usual recoil (see Ross et al. 1978). Ross et al. 1978 and Illarionov et al., 1979 considered the evolution of spectra due to multiple scattering by cold electrons. In the case of neutral hydrogen the additional diffusion term is to be taken into account. This term dominates at $h\nu_1 \lesssim 2keV$. For photon energies $h\nu_1 \gg 2keV$ it can be neglected. Obviously this term is important only for the case of the media, underabundant with heavy elements, when Compton scattering dominates photoionization of the heavy elements (e.g. early Universe at $3 \lesssim z \lesssim 1500$).

b) Transport crosssection

The value of transport crosssection $\int (1 - \cos\theta) d\sigma$, which characterizes the efficiency of changing photon momentum, is important for consideration of spatial diffusion. For atomic hydrogen the transport crosssection is the same as that for free electrons (see above). For molecular hydrogen, helium and heavier elements, coherent (Rayleigh) scattering increases somewhat the transport crosssection (recalculated per one electron). For 2 keV photons the transport crosssection increases by a factor ~ 1.5 , in comparison with scattering by atomic hydrogen or free electrons. With the increase of energy the contribution of the coherent scattering to the transport crosssection falls rapidly.

4. Simple models

We consider below a few situations, where the account for bound electrons can be important. Distortions of spectra are important only when a sharp feature is present in the spectrum. We considered only the case of the iron K_α line, but scattering of other emission lines (e.g. emission lines of helium and hydrogen like ions of heavy elements illuminating a cloud of neutral gas) will lead to similar spectral distortions.

4.1. Monochromatic source in optically thin cloud

All major changes in the spectrum of the radiation scattered by neutral hydrogen can be seen clearly when considering optically thin cloud with monochromatic source in the center. Shown in Fig.4a are the spectra of a scattered 6.4 keV monochromatic line, averaged over all scattering angles ($\equiv \int \frac{d\sigma}{d\Omega dh\nu} d\Omega$) for bound and free electrons.

It is worth mentioning again the similarity of the distortions of the left wing of the line for scattering by hydrogen with distortions appearing for scattering by free electrons in warm plasma with a temperature ~ 10 eV. Shown in Fig.4b is the spectrum of 6.4 keV photons, scattered by free electrons with Maxwellian distribution of momenta with temperatures 0.1, 1 and 10 eV. One can see that with the increase of temperature “blurring” of the left wing also increases. The right side of the line does not change much. Thus in astrophysical conditions the line profile will be always blurred: at low temperatures electrons are bound in atoms and the low frequency wing is blurred due to the distribution of electron momentum in the atom, while at high temperatures electrons are free and blurring is caused by the Maxwellian distribution of electron momentum. Note that in the astrophysical condition (interstellar media, stellar atmospheres, accretion disks) hydrogen is ionized at the temperatures of the order of 1 eV. Therefore “blurring” of a line may be minimal at the gas temperatures $T \sim 1\text{--}5$ eV, when hydrogen is already ionized, but the thermal velocities of electrons are still lower than the typical velocity of a electron in a hydrogen atom.

If the cloud is not uniform or the source is not isotropic then some specific scattering angles will dominate. The spectral shape of the scattered emission changes accordingly. In particular if a compact cloud is illuminated by the emission of monochromatic photons from the distant source, then the recoil spectrum will correspond to the scattering by the given angle (see Fig.3), defined by mutual location of the source, cloud and observer.

4.2. Reflection of continuum spectrum by semi-infinite medium

If the source of X-ray photons has continuum spectrum, then photoabsorption in neutral medium is accompanied by the emission of fluorescent photons in the 6.4 keV line with yield ~ 0.34 per each ionization of the electron from K shell of iron (e.g. Bambinek et al., 1972). The formation of the fluorescent lines of heavy elements (mainly K_α line of iron) due to illumination of neutral medium by the continuum X-ray radiation have been studied in detail in a number of papers (see e.g. Hatchett & Weaver, 1977, Basko, 1978, Bai, 1979, Vainshtein & Sunyaev, 1980, George & Fabian, 1991). Most important astrophysical applications of this problem are: Sun (X-ray continuum is emitted by the Solar flares above the surface of the Sun), normal stars in X-ray binary systems and accretion disks with the hot X-ray emitting region in the center. Note that angular distribution of photons scattered by free or bound electrons is the same and it can be described by the Rayleigh scattering diagram (see above). Thus the results of the calculations of total equivalence width of scattered fluorescent photons should not alter after the account for scattering by bound electrons (note that the contribution from Rayleigh scattering may change somewhat the results of the calculations). At the same time the spectrum and angular distribution of photons, which undergo large recoil, differs strongly. Shown in Fig.8 is the spectrum of the scattered 6.4 keV line, emerging from the semi-infinite plane of neutral matter with a cosmic abundance of heavy elements (the approximation of photoelectric absorption of

Morrison & McCammon, 1983 was used) illuminated by normally incident power law spectrum $F_\nu \sim E^{-\Gamma} phot/s/cm^2$ with slope $\Gamma = 2$. The expression (7) for neutral hydrogen was used as the differential crosssection. The emergent spectrum was averaged over all directions. Note again the “gap” $h\nu_1 - 10.2 \text{ eV} < h\nu < h\nu_1$ and the smeared left wing of the line at the energies $\sim 6.25 \text{ keV}$. For comparison the results of similar calculations with differential crosssection for free cold electrons is shown as a dotted curve. This figure demonstrate the importance of the bound electrons account for the problem of the reflection of X-rays by the atmospheres of the Sun and late stars during strong X-ray flares. Note that the reflection of X-rays takes place at the depth $\sim 1-3 \text{ g/cm}^2$, where the degree of hydrogen ionization is low $\frac{e}{H} < 10^{-3}$ (see e.g. Maltby et al., 1986).

As was expected for cosmic abundance of heavy elements, single scattered photons gives the dominant contribution (see e.g. Basko, 1978,). In the one scattering approximation the spectral shape of scattered radiation can be calculated analytically, using the solution of the double radiation transfer problem by Basko, 1978, which assumes isotropic scattering of continuum photons and neglects change of their energies during scattering. Using the expression (24) of Basko, 1978 and the differential crosssection of scattering by a hydrogen atom we obtain the spectra of single scattered K_α photons (Fig.9). One can see again that the sharp backscattered peak completely disappears.

5. Account for the structure of iron fluorescent K lines and energy resolution of the X-ray detectors

Previous examples deal with monochromatic lines. In order to calculate more realistic spectrum of scattered K_α photons one has to take into account the intrinsic structure of iron fluorescent lines and finite resolution of the X-ray detectors. Two lines (K_{α_1} and K_{α_2}) with energies 6.404 and 6.391 keV and relative intensities 2:1 contribute to the fluorescent emission of iron near 6.4 keV (e.g. Bambinek et al., 1972). According to interpolation of experimental data, the intrinsic width of these lines is ~ 2.65 and 3.2 keV respectively (Salem & Lee, 1976), although theoretical calculations predict somewhat narrower widths $\sim 1.5 \text{ keV}$ (see Salem & Lee, 1976). Shown in Fig.10 are the spectra of the scattered fluorescent emission of iron averaged over all scattering angles. Spectra have been convolved with Gaussian with FWHM=5, 15 and 150 keV in order to demonstrate the impact of the detector resolution on the observed spectrum. It is clear that the predicted distortions of the spectrum could be observed by the instrument with an energy resolution worse than $\sim 15 \text{ eV}$.

6. Some Astrophysical applications

Let us finally consider a few obvious astrophysical applications, where the effects under discussion may be of interest.

6.1. X-ray source in the molecular cloud

Discovery of the giant molecular cloud (Bally & Leventhal, 1991) in the direction of the bright and hard X-ray source 1E1740.7–2942 allows one to assume that the source is surrounded by dense molecular gas. According to the observations at millimeter wavelength the Thomson depth of the cloud can be as high as $\tau_T \sim 0.2$. Sunyaev et al., 1991 noted that if the source is indeed located inside the cloud, then up to 20% of its emission should be scattered by the gas of the cloud. The source 1E1740.7-2942 is strongly variable with the characteristic time scale (according to GRANAT observations) of the order of half a year. In the minimum of the light curve the flux in the hard (35-150 keV) X-ray band decreases by a factor of at least 5-10 (Churazov et al., 1993). This variability significantly increases the chance to observe component scattered by the molecular hydrogen. Obviously along with scattering, neutral gas will absorb X-rays due to photoabsorption and emit fluorescent lines of iron and other heavy elements.

Since optical depth of the cloud for Thomson scattering is large enough, ~ 0.2 , one can hope that with the new generation of X-ray spectrometers it will be possible to observe second order effect - recoil effect due to the scattering of iron K_α photons, borne in the cloud, by the molecular hydrogen. This effect is proportional to the square of the cloud optical depth: up to 20% of the photons in the fluorescent line will be scattered causing a decrease of the photons energies.

Such observations might allow one to determine the position of the source with respect to the cloud and to estimate the total mass of the hydrogen in the cloud. The specific recoil profile demonstrates that we are dealing with molecular or atomic hydrogen. The fraction of the latter is not very high, since no peak of brightness of the 21 cm line has been detected from this direction. Detailed studies of the profile may allow one to measure the abundance of helium in the cloud.

6.2. Galactic Center region

Another apparent example is the region of the Galactic Center as the whole. Ginga observations have shown that central part of our Galaxy contains a bright X-ray source, intensively emitting in the resonance lines of helium-like iron with energies ~ 6.7 keV. The ART-P telescope on board GRANAT localized 5 compact X-ray sources within 100 pc (in projection) from the center of our galaxy, including weak and variable hard X-ray source within 1 arcminute from well known radio source Sgr A* (Pavlinisky, Grebenev & Sunyaev). The map of hard diffuse emission in the GC region, obtained by ART-P (Markevitch, Sunyaev & Pavlinisky, 1993), agrees well with the brightness distribution in the CO molecular line, which reflects the distribution of molecular clouds.

Sunyaev et al., 1993 noted, that such diffuse emission can be due to the scattering of the emission from the compact sources, which have been bright in the past, by the gas in

the molecular clouds, surrounding GC. Obviously if Sgr A or any other compact binary source in this region was emitting 100–400 years ago at the level exceeding 10^{39} ergs/s, then scattering photons will be observed today as diffuse emission. Sunyaev et al., 1993 predicted that if this hypothesis is correct, then molecular clouds should be bright in the neutral iron 6.4 keV fluorescent line.

This prediction has been confirmed by recent ASCA observations (Koyama, 1994), which detected a very bright iron fluorescent line from the direction of the large molecular complexes Sgr B, Sgr A and Sgr C. This leads to the problem of the scattering of K_α photons (originating from the cloud) in the same molecular clouds. In addition ASCA results confirmed the presence of diffuse emission in the resonance lines of helium-like iron with an energy of ~ 6.7 keV. Thus, molecular clouds should scatter emission in resonance lines of strongly ionized iron, which illuminates clouds from outside.

As is known the data on the mass of molecular gas in the GC region obtained from observations of the CO molecule contradict the data on brightness of gamma-rays at the energies of a few 100 MeV originating from interaction of cosmic rays with molecular clouds due to π^0 decay and bremsstrahlung of ultrarelativistic electrons.

The first method of mass estimation is based on the calibration of the CO flux and the amount of H_2 molecules using the nearby clouds and uses observed velocity dispersion and virial theorem (e.g. Solomon, Sanders, Scoville, 1979).

The results of the second method can be agreed with those of the first only assuming that the density of the cosmic rays in the vicinity of GC is an order of magnitude lower than that observed in the disk (Blitz et al., 1985).

With the appearance of a new generation of X-ray telescopes with high sensitivity and energy resolution (AXAF, Spectrum-X-Gamma, ASTRO-E, XMM) observations of recoil profile may become an important source of information on the amount and distribution of atomic and molecular hydrogen in this region.

6.3. Active galactic nuclei

Fine spectroscopy of the active galactic nuclei emission is one of the main goals for the new generation of the X-ray telescopes. As is known, a significant fraction of AGN spectra is characterized by the strong absorption at low energies, which can be interpreted as due to absorption in the molecular torus, surrounding the central source. The Thomson depth of the torus can be of the order or above 1. Since the matter in the torus is neutral, the profile of the lines will be disturbed due to the effects, considered above.

Another important subject is the study of the line profiles, formed in the accretion disks around the galactic nuclei. Doppler shift causes broadening of the line and allows one to use the shape of the line profile for the diagnostic of the matter motion in the disk. Scattering by neutral matter can also contribute to the distortions of the line profile.

6.4. Sun

In principle significant differences in the line profiles for the scattering by hydrogen and helium allows one to make use of these effects for the determination of helium abundance in scattering media. The Sun's surface can be the most important application. Huge flux in the emission lines of the hydrogen- and helium-like ions of iron during powerful solar flares allows one to use fully high energy resolution of new X-ray detectors. Shown in Fig.11 are the typical line profiles, resulting from the reflection of the isotropic flare above the plane surface (Monte-Carlo simulations, resonance line of helium-like iron, 6.7 keV). Photoabsorption due to heavy elements and scattering by atomic hydrogen were taken into account. In real conditions the presence of blends of relatively broad lines will cause additional smearing of the features compared to Fig.11. The most advantageous conditions for such observations take place when angular resolution of the telescope allows one to separate the flare itself and the scattering region. Of interest are profiles of the emission lines of hydrogen or helium ions and K_α emission emerging from the Sun's surface, which is illuminated by the X-ray continuum. The most interesting feature to look for might be the lines resulting from Raman scattering by the neutral helium. In comparison with Fig.11 scattering by helium should lead to additional features at the energies $\sim h\nu_0 - 20$ eV.

6.5. 10^4 K plasma in the vicinity of QSOs and active galactic nuclei

In the vicinity of QSOs and active galactic nuclei plasma clouds may exist with substantial Thomson optical depth, where hydrogen is completely ionized and helium is present in the form of hydrogen-like ions. This opens the possibility to observe scattering by the hydrogen-like ions of helium with the energy gap of 40.8 eV (Fig.12).

Note finally, that the Raman satellite may also appear due to scattering by the elements heavier than hydrogen or helium. The major parameters, determining the strength of the satellites (provided sufficient Thomson optical depth) is the abundance of the given element and the presence of the energy levels, which excitation energy is comparable with the characteristic energy change due to recoil effect. From this point of view young supernova remnants, overabundant with heavy elements may be of special interest.

This work was supported in part by the grants RBRF 96-02-18588-A and INTAS 93-3364. We are grateful to I.Beigman, S.Grebenev, L.Presnyakov, I.Sobelman, J.Truemper and Y.Tanaka for discussions and important comments.

REFERENCES

- Bai T. 1979, *Solar. Phys.*, 62, 113
- Bally J. & Leventhal M., 1991, *Nature*353, 234
- Bambinek W. et al. 1972, *Rev. of Modern. Phys.*, 44, 716
- Basko M. & Sunyaev R. 1973, *Ap&SS*, 23, 117
- Basko M., Sunyaev R., Titarchuk L. 1979, *A&A*, 31, 249
- Basko M. 1978, *ApJ*, 223, 268
- Blitz L., Bloemen J., Hermsen W., Bania T., 1985, *A&A*, 143, 267
- Briggs F., Mendelson L., Mann J., 1975, *Atomic Data and Nuclear Data Tables*, 16, 202
- Bouchet L. et al., *ApJ*, 383, L45
- Churazov E. et al., 1993, *ApJ*, 407, 752
- Eisenberger P. & Platzman P.M., *Phys. Rev. A*, 2, 415
- Eisenberger P., *Phys. Rev. A*, 2, 1679
- Hatchett S. & Weaver R., 1977, *ApJ*215, 285
- Heitler W., 1960, *The quantum theory of radiation*, Oxford, Clarendon.
- Hubbell J. et al., 1975, *J. Phys. Chem. Ref. Data*, 4, 471
- Gummel A. & Lax M., 1957, *Ann. Phys. (N.Y.)* 2, 28.
- George I.M. & Fabian A.C., *MNRAS*, 249, 352
- Koyama K, 1994, *New Horizon of X-ray Astronomy*, FSS-12, 181, Univ. Acad. Press, Tokyo
- Illarionov A., Kallman T., McCray R., Ross R., 1979, *ApJ*, 228, 279
- Landau L. & Lifshitz E., 1958, *Quantum mechanics*, London, Pergamon
- Landau L. & Lifshitz E., 1961, *The classical theory of fields*, London, Pergamon
- Maltby P., Avrett E., Carlsson M. et al. 1986, *ApJ*, 306, 284
- Markevitch M, Sunyaev R., Pavlinsky, 1993, *Nature*, 364, 40
- Mirabel I.F. et al., 1992, *Nature*358, 215
- Morrison R., McCammon D., 1983, *ApJ*, 270, 119
- Pavlinsky M., Grebenev S., Sunyaev R., 1994, *ApJ*, 425, 110

Pozdniakov L. et al., 1979, A&A, 75, 214

Pozdniakov L. et al., 1982, Astrophysics and Space Physics Rev., ed. R.Sunyaev, 1983, v 2,
p. 189, Harwood Academic Publ., Chur

Ross R., Weaver R., McCray R., 1978, ApJ, 219, 294

Salem S.I. & Lee P.L., 1976 Atomic Data and Nuclear Data Tables, 18, 234

Schiff L., 1955, Quantum mechanics, New-York, McGraw-Hill

Schnait P., 1934, Ann. Physik, 21, 9

Solomon P.M., Sanders D.B., Scoville N.Z., 1979, ApJ, 232, L89

Sunyaev R. et al., 1991, ApJ, 383, L49

Sunyaev R., Markevich M., Pavlinsky M., 1993, ApJ, 407, 606

Vainshtein L. & Sunyaev R., 1980, Soviet Ast. Letters, 6, 673

Zombeck M., Handbook of Space Astronomy & Astrophysics, 1990, Cambridge University
Press

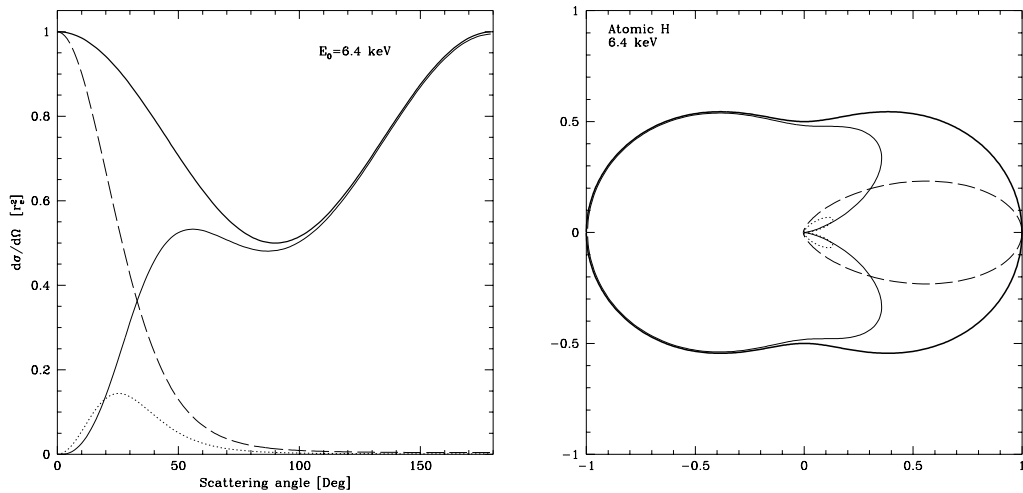


Fig. 1.— Differential cross-section of the 6.4 keV photons scattering by atomic hydrogen as the function of angle. Thin lines show the contributions of Rayleigh (dashed), Raman (dotted) and Compton (solid) scatterings. Thick line shows the cross-section for scattering by a free electrons in the Thomson limit. On the right panel the same values are shown in units r_e^2 . The initial direction of the photon coincides with X-axis.

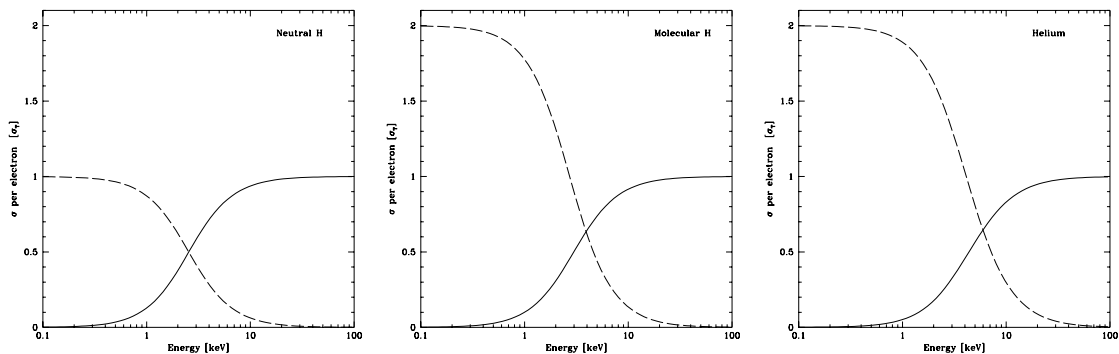


Fig. 2.— a) The contributions of coherent (Rayleigh – dashed line) and incoherent (Raman and Compton – solid line) processes to the total cross-section of photon scattering by a hydrogen atom as the function of photon energy. b) the same as in a) but for molecular hydrogen. c) the same as in a) for helium (using tabulated data of Hubbell et al., 1975)

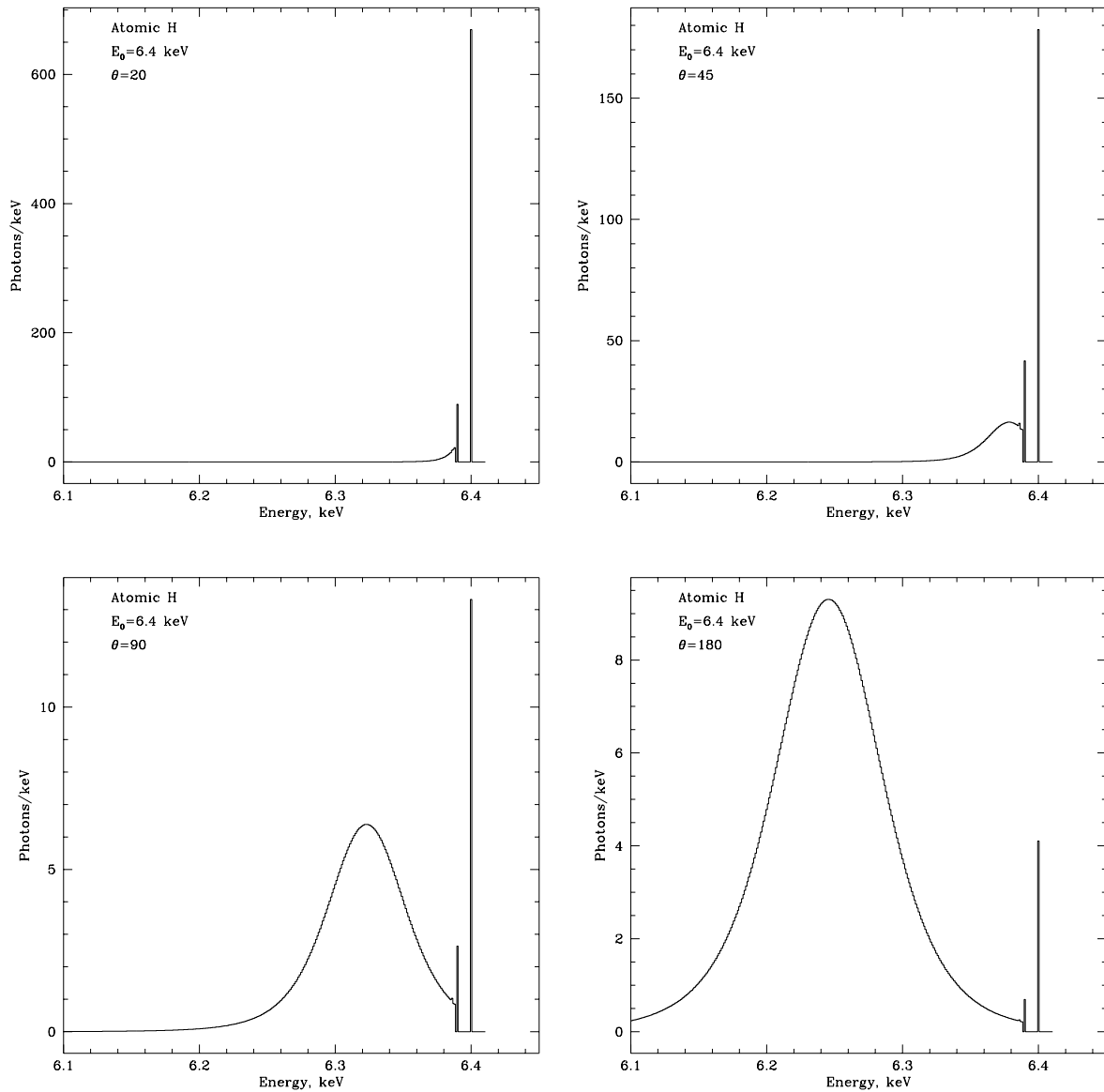


Fig. 3.— Spectrum of the 6.4 keV line as scattered by a hydrogen atom for different scattering angles. The spectra are plotted with 1 eV resolution and normalized on the same line intensity and unit interval over $\mu = \cos\theta$.

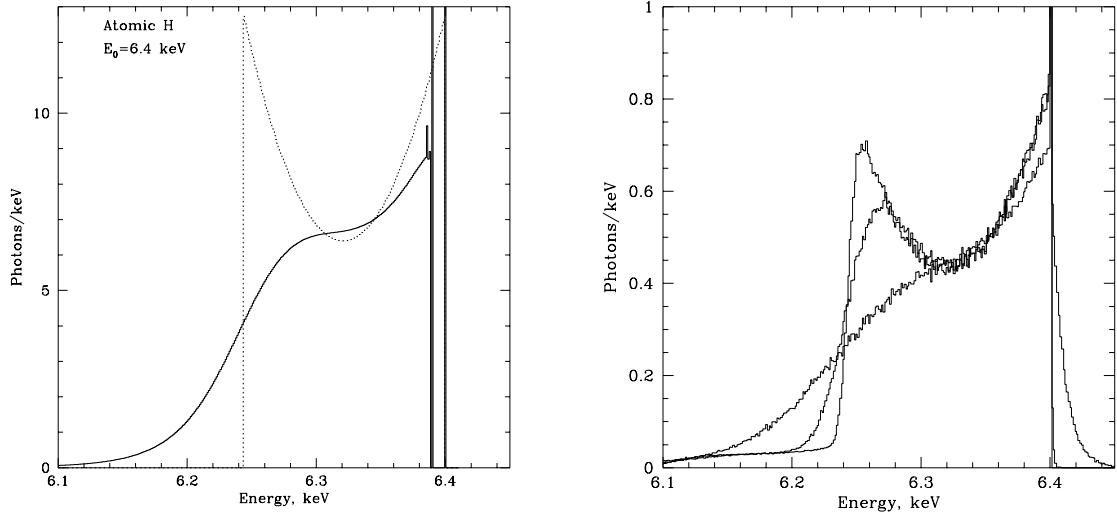


Fig. 4.— a) Neutral hydrogen: Spectrum of the scattered 6.4 keV photons averaged over all scattering angles (solid line). About 13.5 % of photons undergo elastic scattering, 2.3 % of the photons change energy by 10.2 eV – Raman satellite of the line appears, corresponding to the excitation of the second level in the hydrogen atom. The same spectrum calculated for scattering by free cold electrons is shown by the dotted line. b) Emission spectrum emerging from a cloud of free electrons with small optical depth (electron temperatures are 0.1, 1 and 10 eV for three curves respectively). Monte-Carlo simulations.

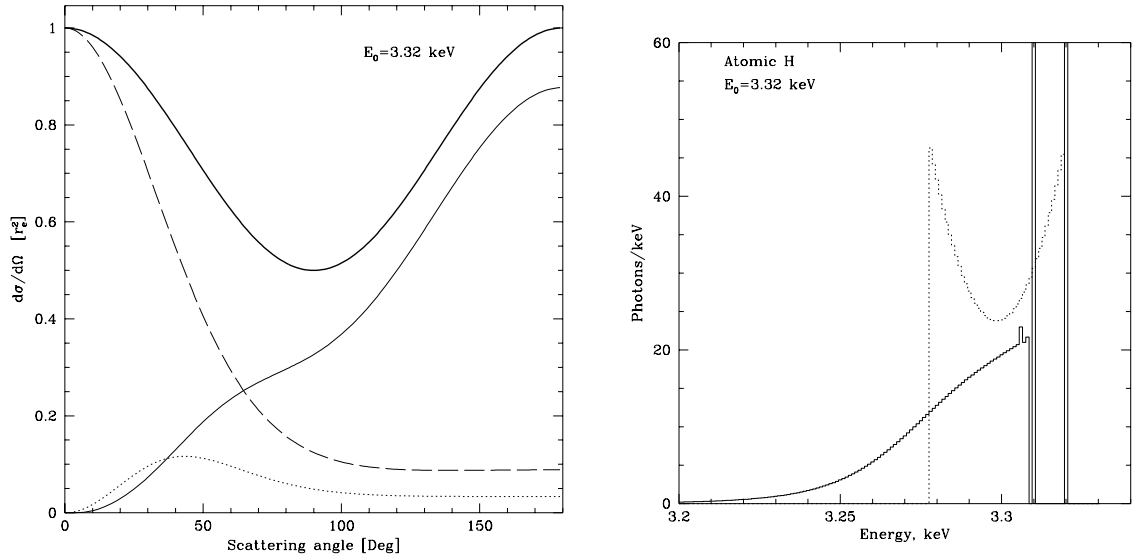


Fig. 5.— a) Differential cross-section for scattering of the 3.32 keV photons by a neutral hydrogen. Thin lines show contributions of Rayleigh (dashed), Raman (dotted) and Compton (solid) scatterings. The thick solid line shows the cross-section for a free electron at rest. b) The scattered spectrum of the monochromatic 3.32 keV line, averaged over all directions. The dotted line shows the spectrum in the case of scattering by free electrons.

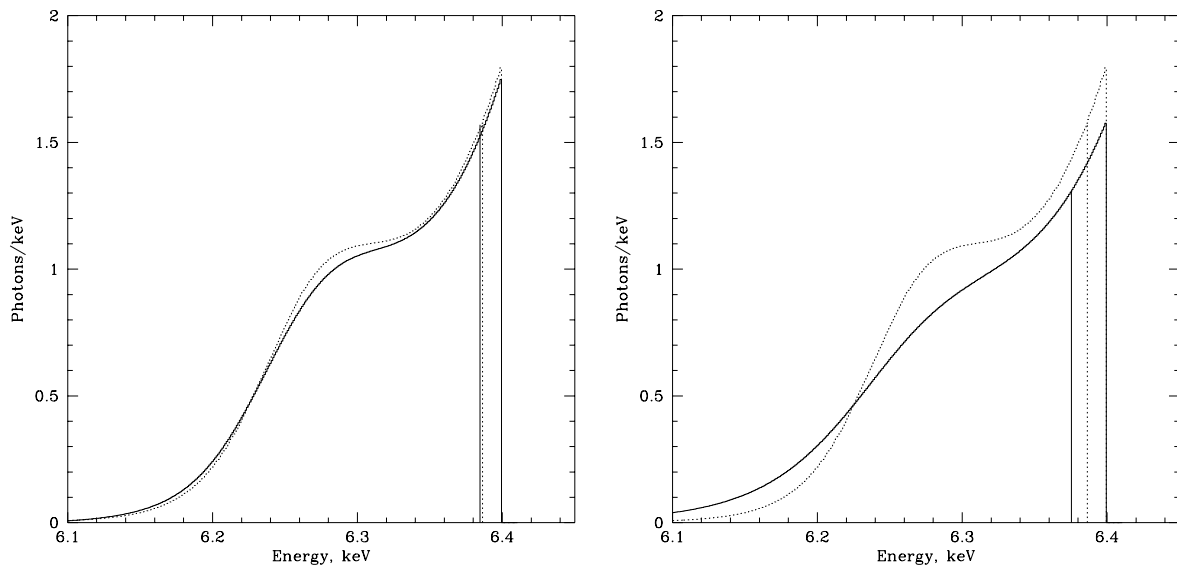


Fig. 6.— a) Spectrum of the 6.4 keV line, scattered by atomic (dotted line) and molecular hydrogen (solid line) and averaged over all scattering angles. b) spectrum of the 6.4 keV line, scattered by hydrogen (dotted) and helium atoms (solid) and averaged over all scattering angles. The spectra have been calculated in “impulse approximation” using the tables of Briggs et al., 1975. Vertical lines to the left of 6.4 keV separate the regions of Compton and Raman scatterings (each line corresponds to the energy $E = 6.4 - E_b$ keV, where E_b is the ionization potential. “Impulse approximation” is not valid to the right of these lines.

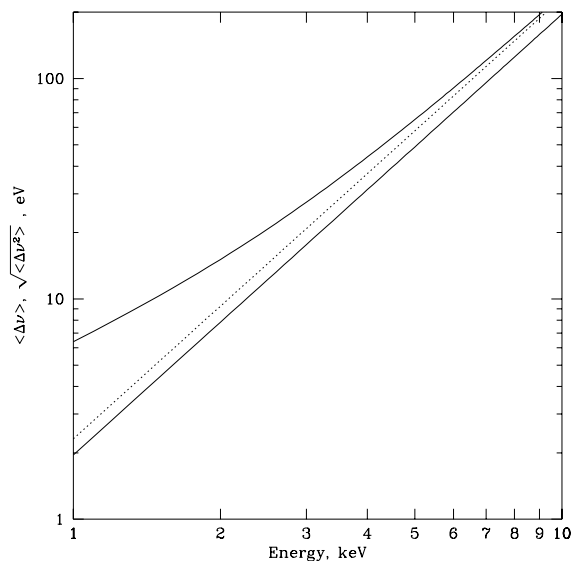


Fig. 7.— Average change of energy (lower line) and square root of average square of change of energy (upper solid and dotted lines) for scattering by free electrons and hydrogen atoms.

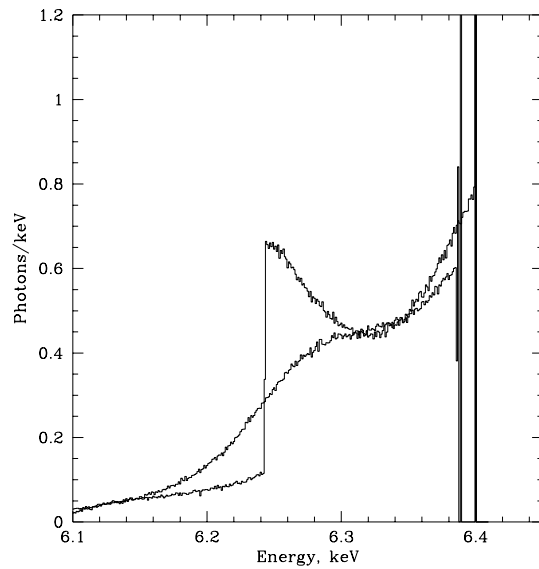


Fig. 8.— Spectrum of scattered radiation in the 6.4 keV fluorescent line of iron, emerging from semi-infinite medium, illuminated by the power law spectrum with the photon index $\Gamma = 2$. The spectrum was averaged over all directions. For comparison similar spectrum for scattering by free electrons is shown. Monte-Carlo simulations.

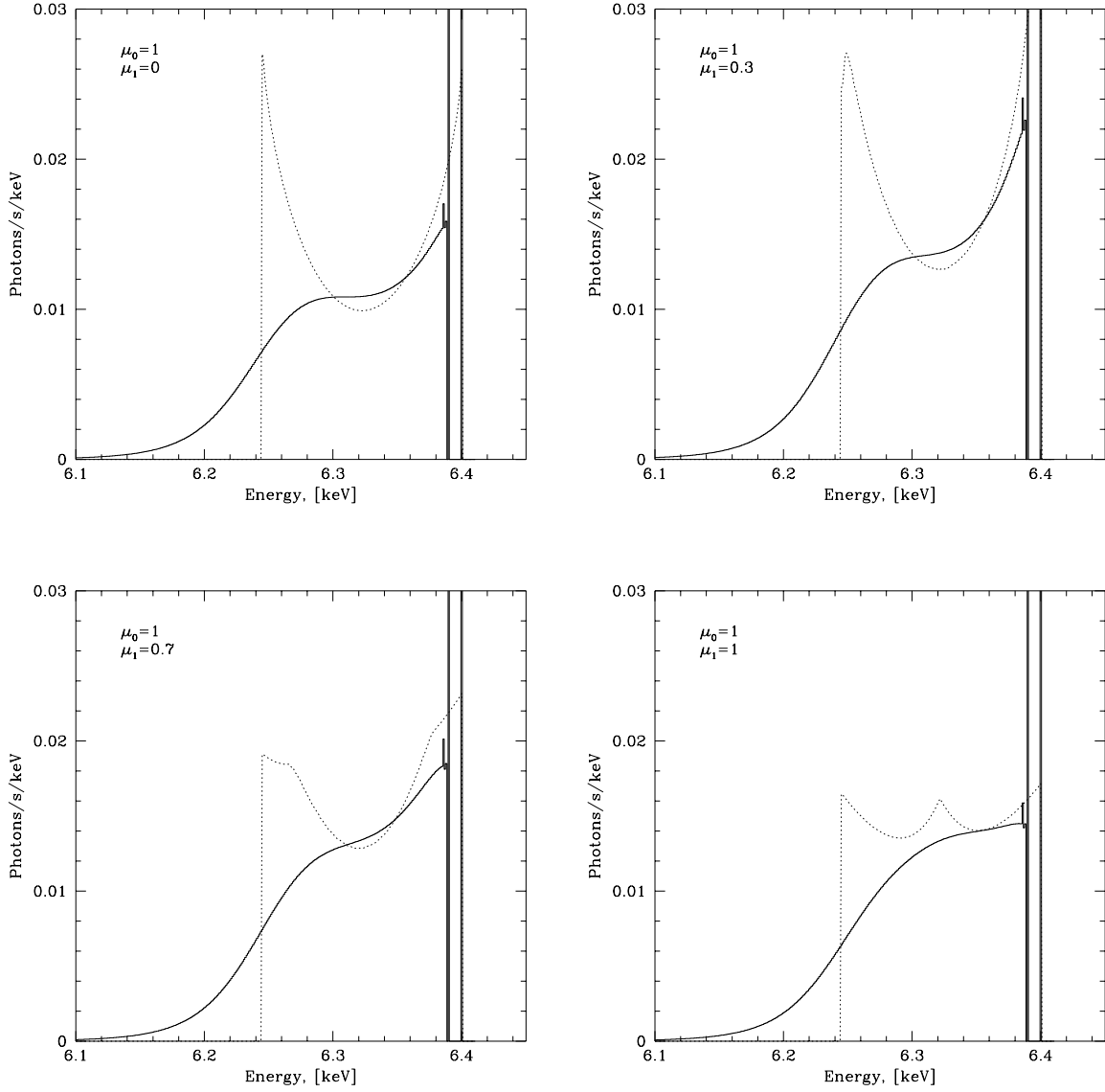


Fig. 9.— Spectra of single scattered radiation in the 6.4 keV fluorescent line of iron, emergent from the semi-infinite media in different directions, illuminated by continuum spectrum. μ_0 , is the cosine of incidence angle for prime radiation with respect to the direction normal to the surface ($\mu_0 = 1$ corresponds to the normal incidence). μ_1 is the cosine of angle between the observer and normal to the surface ($\mu_1 = 1$ corresponds to the photons moving perpendicular to the surface). Analytical approximation.

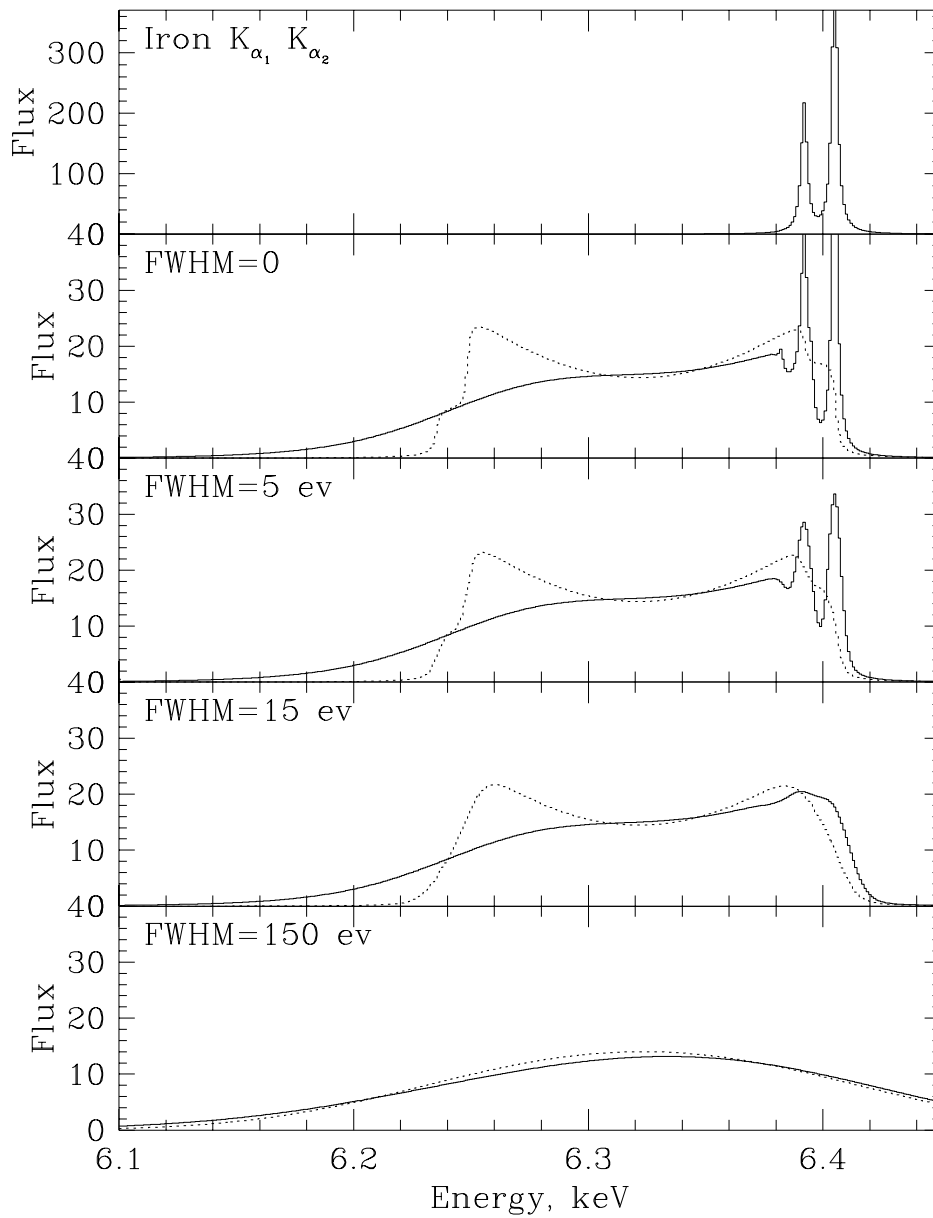


Fig. 10.— Structure of the iron K_{α} lines and predicted spectrum of scattered radiation (averaged over all scattering angles) for different energy resolutions of the detector. Only scattered radiation is shown. The dotted line shows the same spectrum for scattering by free electrons.

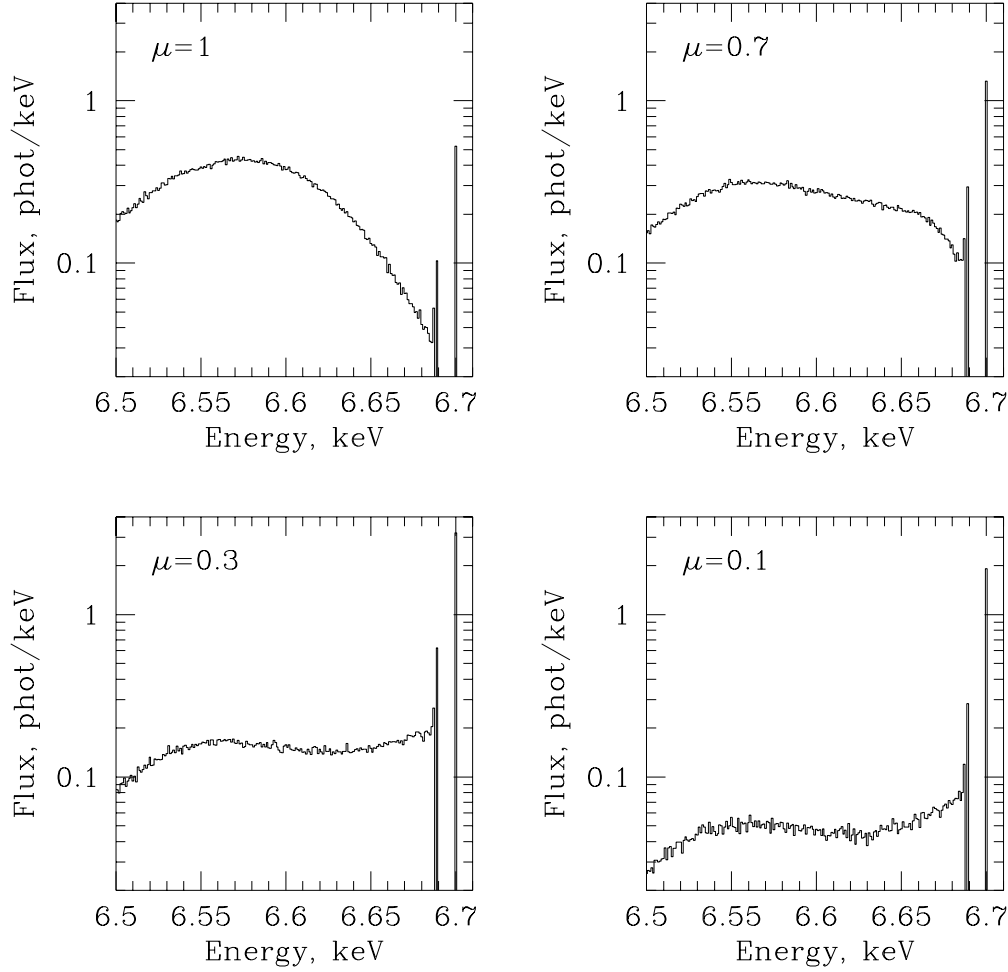


Fig. 11.— Scattered spectrum of the 6.7 keV line, emitted by the isotropic source above the plane semi-infinite media with solar abundance of heavy elements, as the function angle between observer and perpendicular to the surface. μ is equal to the cosine of this angle. In real conditions the presence of several sufficiently broad lines will cause additional smearing of the details seen in the figure.

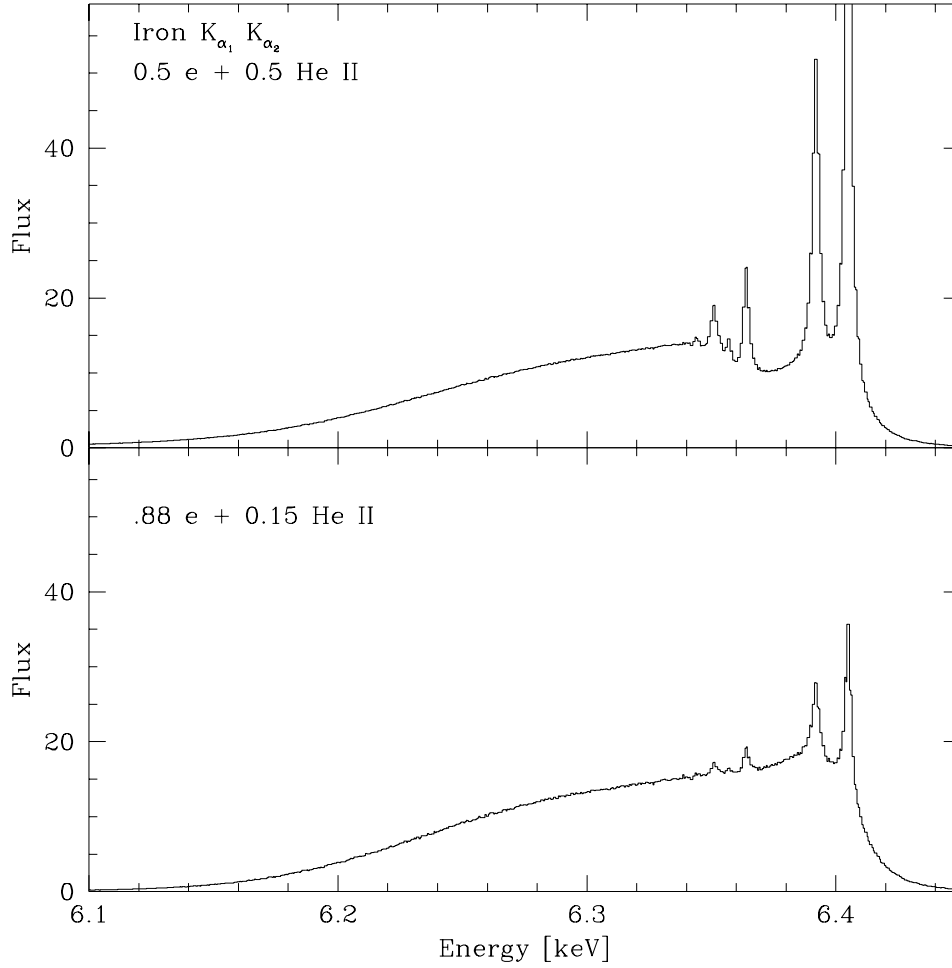


Fig. 12.— Scattered spectrum of iron fluorescent lines by the mixture of free electrons (at $T \sim 10^4$ K) and singly ionized helium, averaged over all angles. For the upper figure fraction of electrons corresponds to the pure helium plasma, for the lower figure fraction of electrons corresponds to the hydrogen plasma with admixture (15%) of helium